Aligned carbon nanotube webs embedded in a composite laminate: A route towards a highly tunable electro-thermal system

Yao, X., Falzon, B., Hawkins, S., & Tsantzalis, S. (2018). Aligned carbon nanotube webs embedded in a composite laminate: A route towards a highly tunable electro-thermal system. Carbon, 129, 486-494. https://doi.org/10.1016/j.carbon.2017.12.045

Published in:
Carbon

Document Version:
Peer reviewed version

Accepted Manuscript

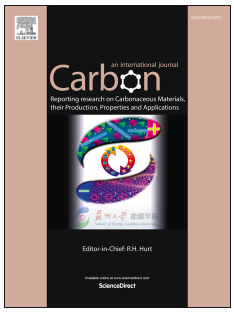

Aligned carbon nanotube webs embedded in a composite laminate: A route towards a highly tunable electro-thermal system

X. Yao, B.G. Falzon, S.C. Hawkins, S. Tsantzalis

PII: S0008-6223(17)31278-2

DOI: 10.1016/j.carbon.2017.12.045

Reference: CARBON 12675

To appear in: *Carbon*

Received Date: 29 October 2017

Revised Date: 9 December 2017

Accepted Date: 11 December 2017

Please cite this article as: X. Yao, B.G. Falzon, S.C. Hawkins, S. Tsantzalis, Aligned carbon nanotube webs embedded in a composite laminate: A route towards a highly tunable electro-thermal system, *Carbon* (2018), doi: 10.1016/j.carbon.2017.12.045.

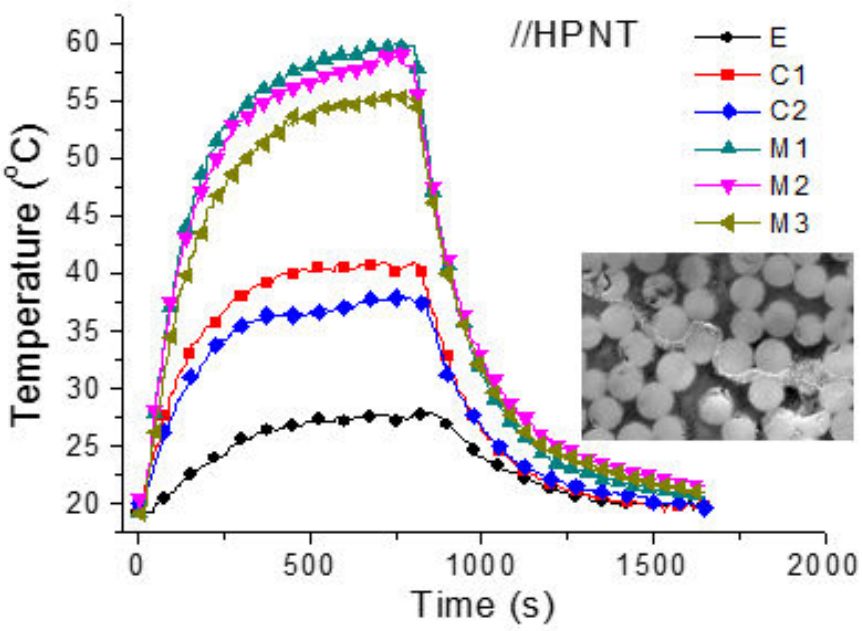
//HPNT
E
C1
C2
M1
M2
M3
Temperature (°C)
Time (s)
60
55
50
45
40
35
30
25
20
0
500
1000
1500
2000

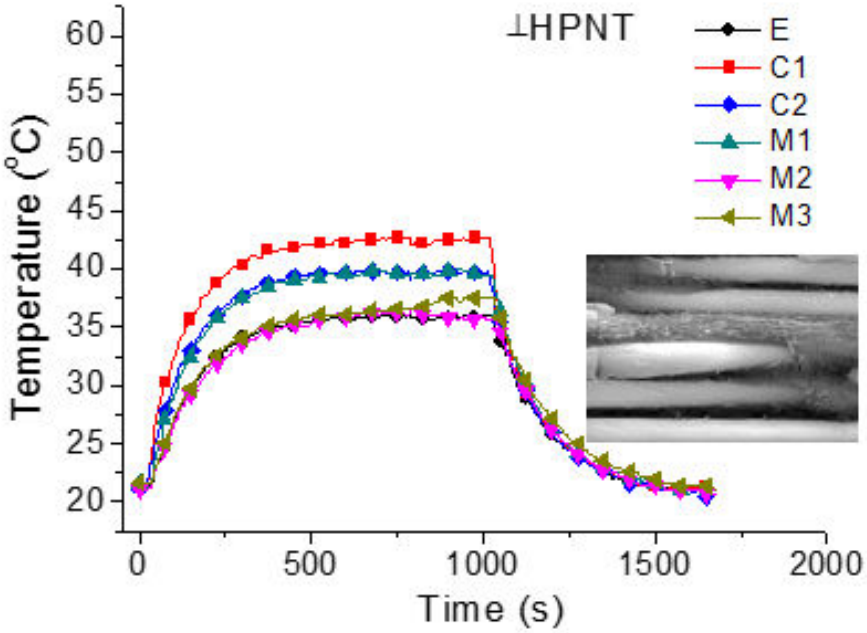
⊥HPNT
E
C1
C2
M1
M2
M3
Temperature (°C)
Time (s)
60
55
50
45
40
35
30
25
20
0
500
1000
1500
2000

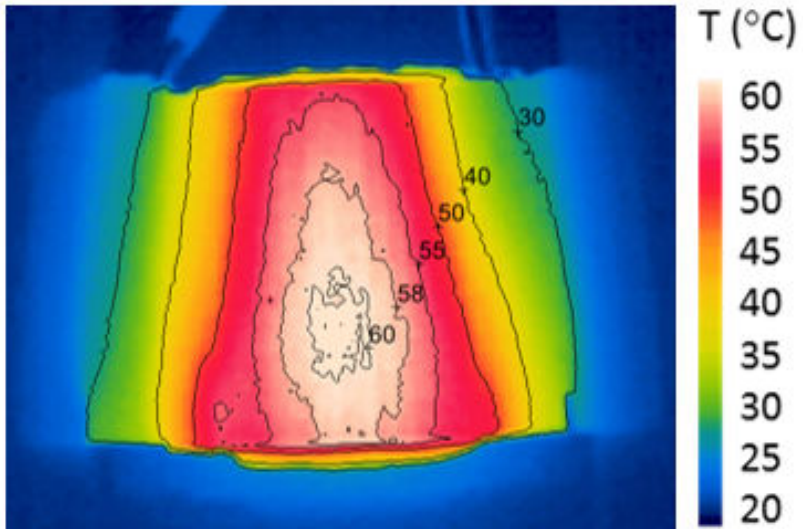
T (°C)
60
55
50
45
40
35
30
25
20
30
40
50
55
58
60

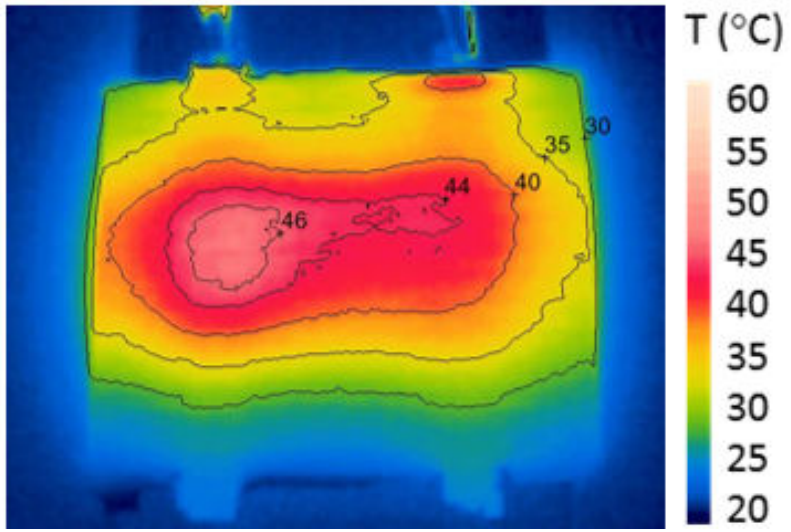
T (°C)
60
55
50
45
40
35
30
25
20
30
35
40
44
46

Aligned Carbon Nanotube Webs Embedded in a Composite Laminate: A route towards a highly tunable electro-thermal system

X. Yao[1], B.G. Falzon[1*], S.C. Hawkins[1,2], S. Tsantzalis[3]

[1]School of Mechanical and Aerospace Engineering, Queen's University Belfast, UK, BT9 5AH

[2]Dept. of Materials Science and Engineering, Monash University, Clayton, Vic., Australia, 3800

[3]Dept. of Mechanical Engineering and Aeronautics, University of Patras, GR-265 00, Greece

*Corresponding Author: Fax: +44 (0)28 9097 4148

E-mail address: b.falzon@qub.ac.uk (B.G. Falzon)

Abstract

Highly aligned CNT webs, with an areal density of 0.019 g/m^2, were produced by direct drawing of CNT 'forests' grown by chemical vapor deposition, to form a conductive heating element. These were subsequently inserted between pre-cured layers of unidirectional carbon fibre reinforced polymer (CFRP) and the electrical and thermal conductivity of the combined system were assessed under different curing conditions. Control composites specimens, cured under high-pressure, demonstrated a higher fibre volume fraction, as well as higher electrical and thermal conductivities. With a single CNT 20-layer web interlayer added, the electrical conductivity increased by 25% when the CNT web alignment was perpendicular to that of the fibres, and by 15% when the CNT web alignment was parallel to the fibres. In addition, three types of CNT interlayer distribution were investigated. Through tailoring the pressure, carbon fibre layup and CNT interlayer, an efficient electro-thermal system was obtained which could be deployed as part of an ice-protection system on aircraft.

1. Introduction

As an aircraft flies through clouds at temperatures below 0 °C, super-cooled water droplets may impinge upon vulnerable aerodynamic surfaces and accumulate as ice, especially on the leading edges of wings, fins, tails, jet intakes or propellers [1]. Ice accretion adds weight, increases drag, and may significantly reduce lift, leading to a complete loss of control [2]. Ice accretion has been a contributing factor in 9.5% of fatal air-carrier accidents [3], and has consequently attracted considerable research interest aimed at developing energy-efficient anti-icing (AI) and de-icing (DI) systems.

Carbon fibre reinforced polymer (CFRP) composites have become the predominant material on the primary structure of the latest generation of passenger aircraft, owing to their superior specific strength and stiffness compared to traditional metallics. In the latest generation of wide-body passenger aircraft, e.g. Airbus A350 XWB and Boeing 787, more than 50 wt% [4] CFRP composite has been utilised in their primary structure. However, the relatively low thermal conductivity and the ever-greater emphasis on energy efficiency, demand a new approach to prevent ice accretion on susceptible aerodynamic surfaces. One of the most widely used anti-icing/de-icing (AI/DI) techniques is the hot-air-bleed system. The air is bled from the engine compressor stages, piped to vulnerable areas and expelled through small holes to the inner surface of the leading edge skin to heat the outside surface by thermal conduction [5,6]. As CFRP composites have much lower thermal conductivity compared to metals, more hot air is required, leading to higher thermal losses and energy consumption. In addition, air-bleed decreases the efficiency of the engines, and the piping network adds weight and maintenance costs [7].

In recent years, diverse ice protection systems have been investigated, including electro-thermal systems [6–12], electro expulsive systems [13], superhydrophobic coatings [14–16] and flexible pneumatic boots [17]. Among these, an electro-thermal system can be used for both anti-icing and de-icing, where a moderately conductive foil or wire element is commonly embedded in the critical surface and resistively heated. As current passes through the element, the heating weakens the bonding between the ice and impinged surfaces and the ice is consequently dislodged by the airflow [18]. The electrical heating element is the key component for this system. Metal is currently used for this function (eg. Boeing 787) but suffers from bonding, weight and heating uniformity problems [19]. As a consequence, alternative materials have been investigated, including carbon nanotubes (CNTs) [6,9–11,20–25], carbon fibre (CF) [12] and electro-conductive textiles [7].

Although CNTs possess excellent electrical conductivity at the individual level, macroscopic constructs of CNTs entail innumerable resistive contacts which can be utilized to produce an electro-thermal heating element. The macroscopic magnitude of the resistance can be tailored by functionalization but also, and more readily, by varying the amount or concentration of CNTs with virtually no weight penalty, given their vanishingly small mass. This, together with their exceptional specific strength and stiffness and compatibility with CFRP composites allows CNT heaters to be designed and shaped to optimize energy use to achieve anti-icing/de-icing while maintaining the structural integrity of the CFRP composite structure.

Dispersed CNTs have been widely investigated as the heating element [10,20,21], and applied through different methods. However, as dispersed CNTs present numerous challenges, such as achieving uniform dispersion, and difficulty in tuning for specific properties, aligned CNTs have emerged as potential efficient heating elements. Janas and Koziol et al. [22,23] have

developed CNT films and CNT wires, which were directly spun from an aerogel produced by chemical vapor deposition (CVD) and continuously deposited onto a rotating winder [26]. However, the resulting CNT assemblies have high loading of catalyst and amorphous carbon as well as disordered CNTs. Wardle et al. [6,9,24] conducted research on the electro-thermal properties of a heating system with aligned 'knocked-down' CNTs as the heating element, and proposed a thermal-mechanical de-icing system which employed aligned CNT as the heating element. Knocked-down CNTs are obtained through pressing down and shearing aligned CNTs in one direction. As a result, there is very little that can be done to adjust the resistance. Fuzzy fibres [27], i.e., growth of CNTs on CF fabrics, is attractive for some applications but entails both extensive processing and often significant damage to the CF performance.

A uniquely useful form of high purity, highly specified CNT material is as 'directly drawable forests' of CNTs grown on a substrate such as silicon wafer, achieved through a carefully controlled CVD process [28] available within the Advanced Composites Research Laboratory at the Queen's University Belfast. Many other CNT products are heavily loaded with iron or other catalysts. Leaving the catalyst in place can result in gradual oxidation, leaching, and incompatibility between the CNTs and CFRP composites, however methods used to remove it are onerous and can damage and tangle the CNTs in the process. In contrast, directly drawable CNTs are essentially catalyst-free and require no purification. A fine, continuous film or web of CNTs can be drawn horizontally from the vertically aligned forest and used as-formed or laterally condensed into yarn [29]. The web is typically only around 50 nm thick when densified, has an areal density of approximately 2 $\mu g/cm^2$ and the CNTs are highly aligned and conductive along the draw direction.

As illustrated by Musameh et al [30], the resistance of a laminated CNT web decreases inversely to the number of layers. Also, within a single web, the length of CNTs can be controlled during the CVD procedure. Accordingly, by controlling these three parameters (number of layers, orientation and length of CNTs), the desired electro-thermal properties of the CNT web can be achieved. Directly drawn carbon nanotube (CNT) web is a promising alternative to metal heating elements in that it adds very little weight, is compatible with composites and indeed may contribute to the structural performance, and, being highly anisotropic, flexible and adaptable, offers exceptional flexibility in design and fabrication to optimize performance. In this work, heating elements comprising CF laminates alone and in combination with interlaid CNT web are investigated. The effects of curing pressure on CFRP composite fibre volume fraction, resistance and thermal conductivity, with and without CNT web interlayers, as well as the effects of different CNT layer morphologies, are discussed.

2. Experiments

2.1. Materials

Aerospace grade IM7/977-2 carbon fibre/epoxy unidirectional prepreg (Cytec/Solvay), was used in this work. The CNT forests were fabricated by CVD of acetylene at 700 °C, grown on a silicon wafer with iron catalyst [28,29]. The obtained CNTs, with an average length of 300 μm, and an average diameter of 10 nm (Fig. 1a), were drawn directly into a fine continuous web of aligned CNTs and wound onto mounting frames (Fig. 1b) to the required thickness. As noted [30] the resistance of CNT web falls in inverse proportion to the number of layers (ie two layers have half the resistance of one, and twice the resistance of four). Web comprising 20 layers of CNT, wound as a single sheet or as multiple sheets summing to 20 layers, was chosen for this investigation. Strips of 10 mm wide copper foil (Alfa Aesar, 0.025 mm thick,

annealed, uncoated, 99.8%) were used as the electrical buses to connect samples and power supply.

2.2. Sample preparation

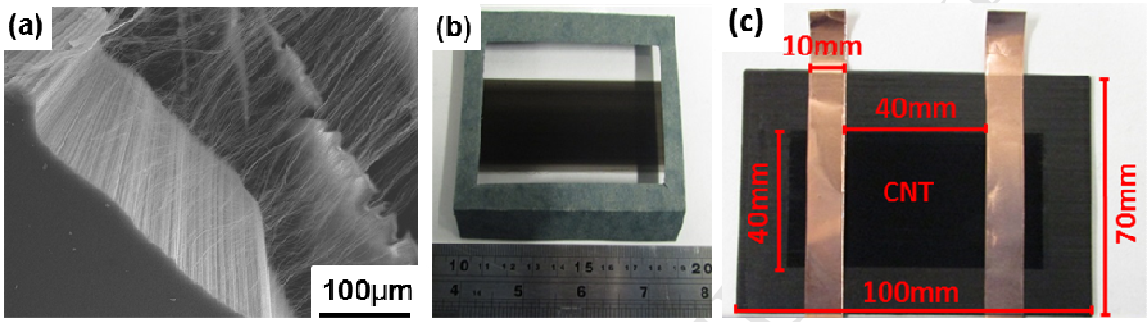

Fig. 1. (a) SEM image of drawable CNT forests (b) CNT web on mounting frame (c) Sample dimensions.

Table 1. Sample test matrix

Specimen Type	CF layer	CF direction	Platen curing pressure (bar*)	CNT web (layer)
//HP	18	90°	7	0
//LP	18	90°	0	0
⊥HP	18	0°	7	0
⊥LP	18	0°	0	0
//HPNT	18	90°	7	20
⊥HPNT	18	0°	7	20

*Note: Excludes -1 bar vacuum pressure and closing pressure of press at zero nominal applied pressure.

Composite laminates (100 mm × 70 mm), made of 18 plies of prepreg were cured at 177 °C for 3 hours using a platen press (COLLIN P200P), combined with vacuum. Copper buses were placed 40 mm apart between plies 9 and 10 to create a heater area of 40 mm × 70 mm (Fig. 1c). Specimens with carbon fibre (CF) perpendicular (⊥) or parallel (//) to the buses were made under high ('HP') and low ('LP') curing pressures (Table 1). HP samples with CNT web (denoted 'NT'', one web comprising 20 layers) placed perpendicular to the buses (Fig. 1c) and embedded in the middle of HP samples were also prepared. Subsequently, the effect of CNT webs placed as two webs each of 10 layers, or 5 webs of 4 layers was studied (Fig. 7). The buses are all in the middle, i.e. with 9 layers of CF on each side.

2.3. Characterization

A Hitachi FlexSEM1000 Scanning Electron Microscope (SEM) was used to observe the morphology of CNTs and cross section of the specimens. Thermogravimetric analysis (TGA, TA Instruments SDT-Q600) was used to find the fibre volume fraction and an Agilent 34450A 5½ Digital Multimeter to measure the resistance of the samples using the 4-wire method. Thermal conductivity of the samples was measured by a TC analyzer (TCi Mathis) using a modified transient plane source (MTPS) technique. In this test, the heat generated by the heating element of the sensor, with a known applied current, yields a temperature rise, at the interface between the sensor and the sample, which causes a change in the voltage drop of the sensor element. The rate of the voltage rise is used to determine the thermal conductivity of the sample. Before the thermal conductivity measurement, the surface roughness, R_a, of the samples was reduced by sanding to less than 1 μm for a more uniform contact between sensor and specimen surface.

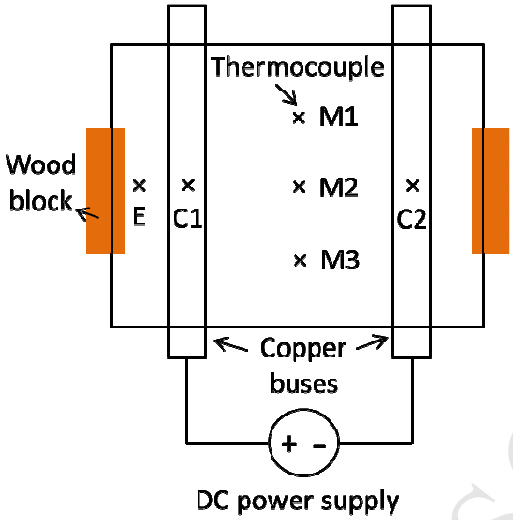

Fig. 2. Sample thermal testing setup and thermocouple location.

The resistive heating performance of the composites, including temperature vs. time and temperature distribution, were investigated. The current was supplied by a DC power supply, and the temperature of the samples recorded by RS-1384 4 Input Data Logging Thermometers using K-type thermocouples (TCs) (Fig. 2). Six thermocouples were placed at different locations on the sample, three in the middle (M1, M2, M3), two on the copper buses (C1, C2) and one near the edge (E). Furthermore, the temperature distribution was monitored by an FLIR i60 thermal imaging camera, with image frequency of 9 Hz and IR resolution of 180 × 180 pixels. The sample was placed over two wooden blocks, as indicated in Fig. 2 in a still air environment at ambient temperature.

3. Results and discussion

3.1. Effect of curing pressure on CFRP fibre volume fraction

Curing pressure has a significant effect on the fibre volume fraction and hence the

conductivity and mechanical performance of CFRP composites. In this study, samples were held under a dynamic vacuum of -1 bar and processed at a nominal platen pressure of either 7 bar or zero bar. (Table 1). Fibre weight fraction (w_f) was obtained through TGA (Fig. 3).

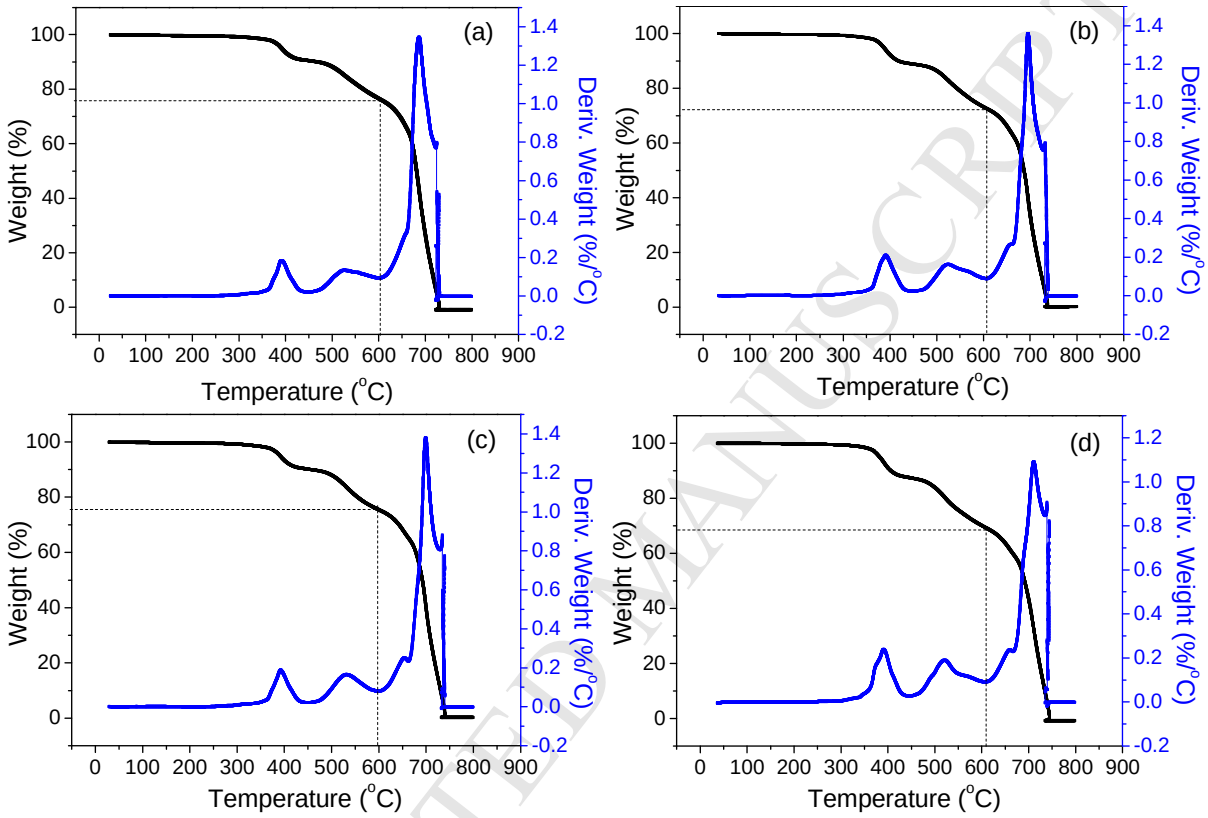

Fig. 3. TGA curves of sample (a) //HP (b) //LP (c) ⊥HP (d) ⊥LP.

Table 2. Fibre volume fraction of the samples

Specimen Type	ρ_c (g/cm^3)	ρ_f (g/cm^3)	W_f (%)	V_f (%)
//HP	1.558	1.78	76.62	67.06
//LP	1.509	1.78	72.67	61.61
⊥HP	1.555	1.78	75.79	66.19
⊥LP	1.524	1.78	69.61	59.60

The weight fraction, w_f was converted to volume fraction V_f [31] using,

$$V_f = W_f * (\rho_c / \rho_f), \quad (1)$$

where the density of CF is known (ρ_f =1.78 g/cm^3) and the density of the composite (ρ_c) can be determined (m_c / V_c). Each sample was cut from the middle to obtain a rectangle with a size of approximately 3 cm x 4 cm, then sanded and the edges polished to make them smooth and straight to calculate the volume and density. The TGA analysis (Table 2) shows that CF//Cu and CF⊥Cu samples manufactured under high-pressure have 8.8% and 11.1% higher fibre volume fractions respectively than their low pressure counterparts.

3.2. Effect of curing pressure and insertion of CNT web interlayer on CFRP resistance and thermal conductivity

The resistance varied between samples under different curing pressures and CF orientation, with higher pressure (and hence higher fibre volume fraction) giving a reduction in resistance of 36% to 22.3 Ω for the CF//Cu orientation and 96% for the CF⊥Cu sample from 3.45 Ω to just 0.13 Ω (Table 3). This reflects both the improved CF to CF and CF to Cu bus contact with lower resin content and also the conduction along the CF fibres rather than across them for the perpendicular and parallel orientations respectively. Inclusion of only one CNT web (20 layers) within the HP sample reduced resistance by 25% for the CF//Cu samples and by 15% (to 0.11 Ω) for the CF⊥Cu samples.

A higher cure pressure resulted in an increase of ~11% in thermal conductivity (k) for both CF⊥Cu and CF//Cu samples as the carbon fibres, which have higher intrinsic thermal conductivity than the resin, come into closer contact. As the laminar resistivity is the

dominant part of the thermal resistivity [32], with the curing pressure increased, the laminate thickness as well as the interlaminar interface thickness decreased, resulting in a decrease in the thermal resistivity of the specimen. Similarly, CF//Cu samples possess higher thermal conductivity owing to their higher fibre volume fraction compared with the CF⊥Cu samples. Inclusion of a single 20 layer CNT web at the centre of 18 CF plies does not appear to significantly change the thermal conductivity (see section 3.4).

Table 3. Effect of CF-Cu bus orientation, cure pressure and CNT addition on the electrical and thermal conductivity of 18 ply CFRP composite.

Sample (*)	**Cure Pressure**	**CF Orientation to Cu Bus**	**CNT Interlayer**	**Electrical Resistance, Ω**	**Thermal Conductivity, W/m·K**
//LP	Low	//	-	34.7±2.13	0.650±0.022
//HP	High	//	-	22.3±0.39	0.722±0.015
//HPNT	High	//	√	16.7±0.51	0.764±0.005
⊥LP	Low	⊥	-	3.45±0.06	0.639±0.039
⊥HP	High	⊥	-	0.13±0.02	0.707±0.011
⊥HPNT	High	⊥	√	0.11±0.02	0.707±0.011

*Note: e.g. //HPNT represents specimens with carbon fibres parallel (//) to the buses made under high curing pressures (‘HP’) with one 20 layer CNT web (‘NT’) embedded.

3.3. Resistive heating performance

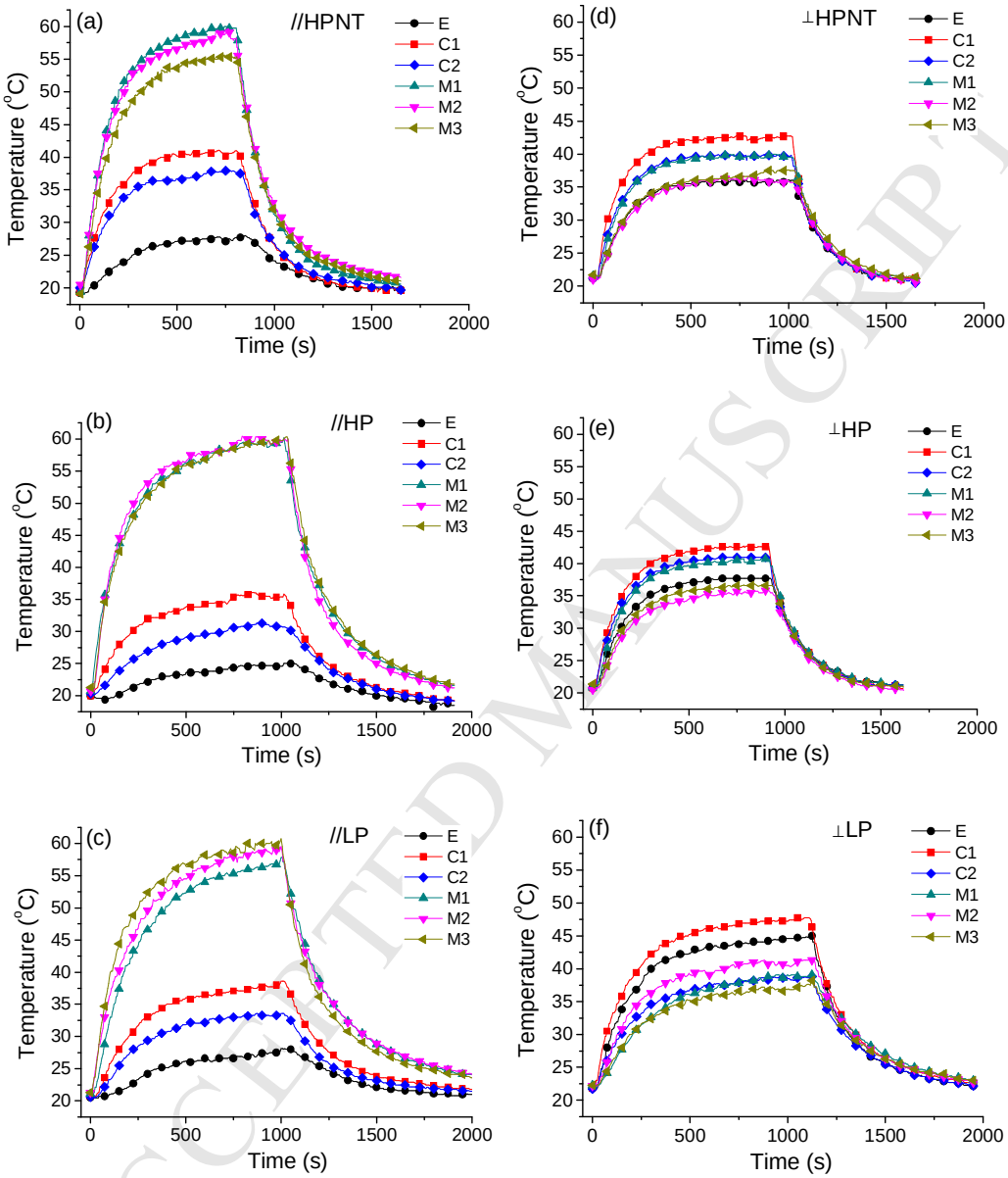

Fig. 4. Temperature variation at six positions (Fig. 2) recorded by TCs at a constant input power of 4.8 W of sample (a) //HPNT (b) //HP (c) //LP (d) ⊥HPNT (e) ⊥HP (f) ⊥LP

The same input power, 4.8 W, was applied to all samples (by adjusting the input voltage and current) via the copper bus, and the temperature, heating and (following cessation of heating) cooling pattern as a function of time were recorded (Fig. 4). For CF//Cu samples, the middle

zone of the specimens (TCs M1, M2, M3 (Fig 4a-c, also see Fig. 2)), exhibit the highest temperatures as the current must travel between the buses by crossing from CF to CF. The specimen resistance is thus mainly due to CF – CF contact. This is much higher than the CF – Cu contact resistances which do not heat up as strongly (TCs C1, C2 Fig 4a-c). Furthermore, as the thermal resistance along CF is much lower than across a CF specimen, where heat must also move from one fibre to the next, the area between the buses heats relatively uniformly but heat cannot spread readily outside this zone (TC E, Fig. 4a-c). For CF⊥Cu samples, current travels from one bus to the other along the carbon fibre and hence the sample resistance is low. The contact resistance between CF and Cu is comparable to the sample resistance, so the buses heat up as well (Fig. 5h). Therefore, TC points C1 and C2 have the highest temperatures (Fig 4d-f) and the section outside of the heated zone (ie TC E) also becomes hot. The broader distribution of heat for the same energy input results in a lower maximum temperature for the given power consumption.

To better understand the heat generation and transfer process, an infra-red camera was used to observe the performance of //HPNT and ⊥HPNT samples (Fig. 5). The pictures were taken 90 s after commencement of heating (Fig. 5a,b); at steady state after heating for 300 s (Fig. 5c,d); and 60 s after heating was ceased (Fig. 5e,f). For CF//Cu samples, the area between the electrodes heats quite uniformly as heat is transferred efficiently parallel to the copper buses but not across them to the outer edges of the sample (Fig. 5a,c,e,g). Thus, the heat dissipation area is essentially only that between the electrodes, or approximately 42 cm^2 which, at the input power of 4.8 W, gives a power density of 1143 W/m^2. In contrast, for CF⊥Cu samples heat is transferred along the fibres and across (and along) the copper buses to the whole sample, a dissipation area of 70 cm^2 and a power density of only 686 W/m^2. This accounts for

the ~40% lower temperature increase seen for CF⊥Cu samples (Fig. 4). In addition, the lower resistance of the ⊥HPNT sample makes the CF-Cu contact resistance more significant so excessive heating occurs at those locations (Fig 5b,d,f,h).

Sample //HPNT **Sample ⊥HPNT**

After heating for 90 s

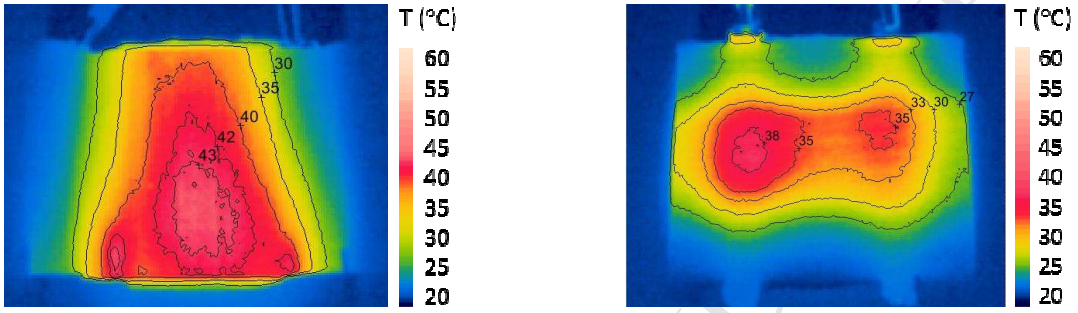

(a) (b)

Steady state – after heating for 300s

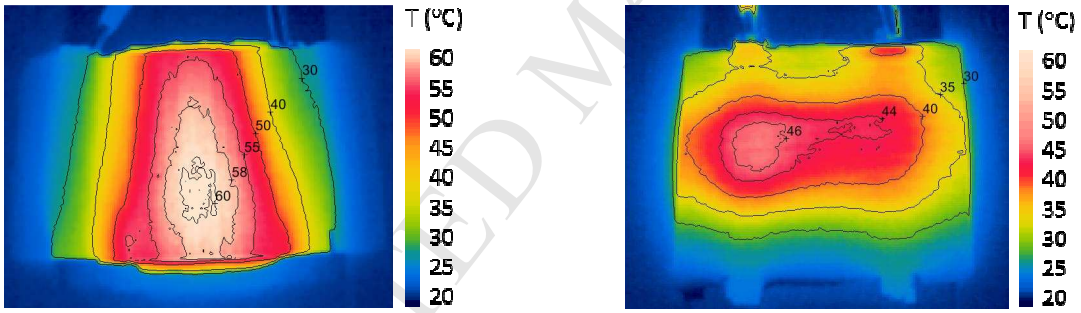

(c) (d)

60s after heating ceased

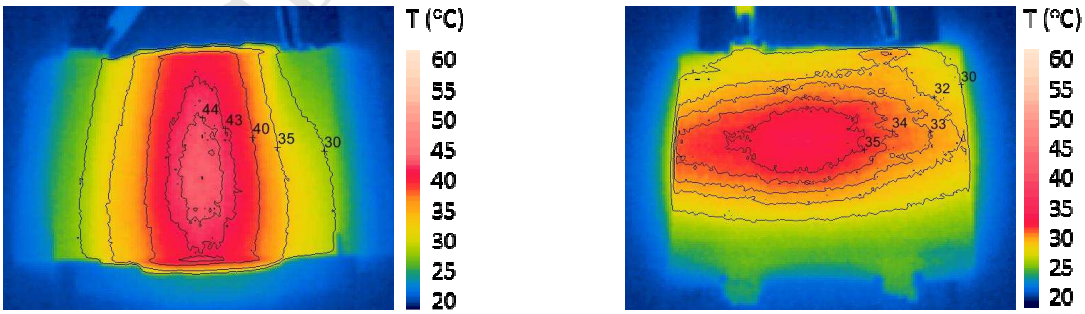

(e) (f)

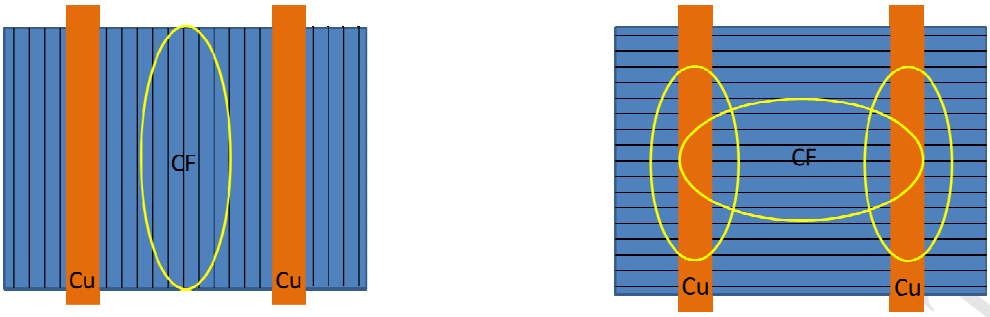

(g) (h)

Fig. 5. IR images of sample //HPNT (a, c, e) and ⊥HPNT (b, d, f), captured at ambient room temperature, and the corresponding schematic of samples (g, h, yellow ovals represent the heat concentration areas).

3.4. Effect of the distribution of CNT web interlayers

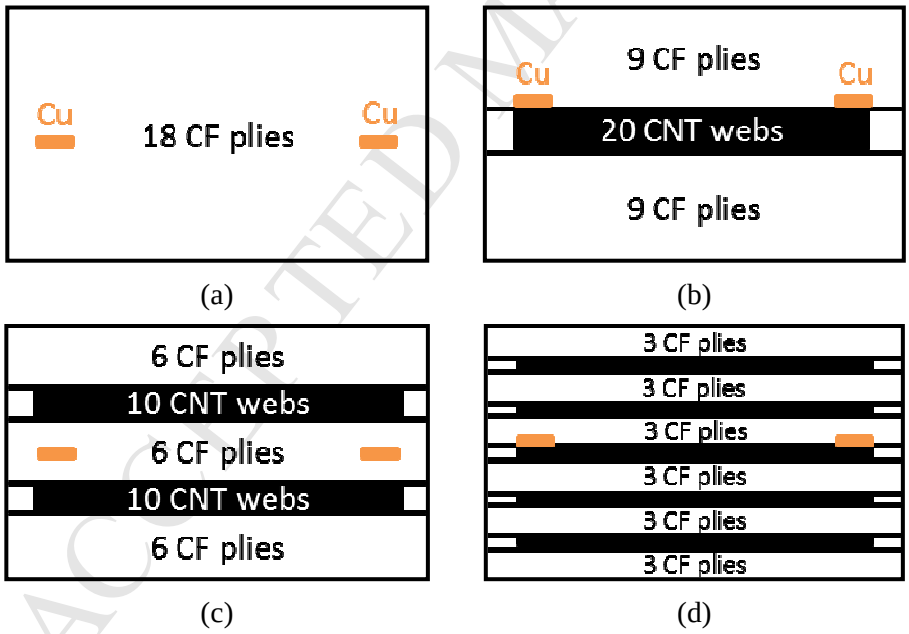

(a) (b)

(c) (d)

Fig. 6. Samples with different CNT web interlayer distributions, (a) without CNT web as the control sample, with interlayers comprising (b) one 20 layer CNT web, (c) two 10 layer web and (d) five 4 layer web.

In order to study the relationship between the web location and composite device's performance, three different CNT web interlayer distributions were applied to the CF/epoxy composites whilst maintaining a total number of 20 layers, as indicated in Fig. 6. The resulting electrical and thermal properties are summarized in Fig. 7. The electrical resistance (Fig. 7a) of all CF⊥Cu samples is lower compared with the corresponding CF//Cu samples as the current flows along the carbon fibres easily and insertion of CNT web has only a very slight effect. In contrast, addition of CNT web significantly lowers the resistance of the CF//Cu samples (Fig. 7a) especially for the samples with 20 CNT interlayer or 5 x 4 CNT interlayers (Fig. 6b,d) in which the CNT interlayers contact the copper buses directly. Unlike the electrical conductivity, the thermal conductivity is only slightly if at all affected by the presence and distribution of the CNT web interlayer (Fig. 7b). The CF//Cu samples all have higher thermal conductivity than the CF⊥Cu samples, consistent with the higher fibre volume fraction of the former (Table 2, 3).

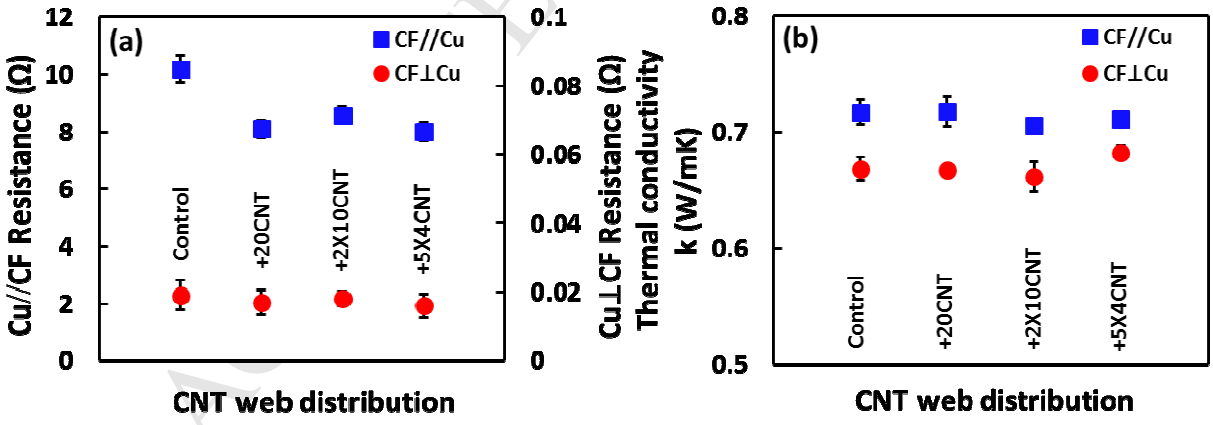

Fig. 7. (a) Electrical resistance and (b) thermal conductivity of samples with different CNT web interlayer distributions

The difference between the trends in thermal and electrical conductivity is related to their conduction modes. CFRP composites are solids with crystalline structures, and their heat conduction mainly depends on the energy transfer by molecular and lattice vibrations in the form of phonons. Phonon interactions include phonon-phonon scattering (normal process and umklapp process), phonon-defect scattering and phonon-boundary scattering, and the umklapp process contributes to the thermal resistance [33]. The thermal conductivity is related to the value of the mean free path of phonons. Although the embedded CNTs have higher thermal conductivity and will provide more thermal pathways, composites with different dispersion of CNT web interlayers represent similar thermal conductivities. This could be explained in two ways as, on one hand, the CNT web interlayers will also lead to the phonon scattering at the innumerable CNT – CNT and CNT – CF junctions. On the other hand, compared with the content of carbon fibre and epoxy, the mass of CNT is negligibly small.

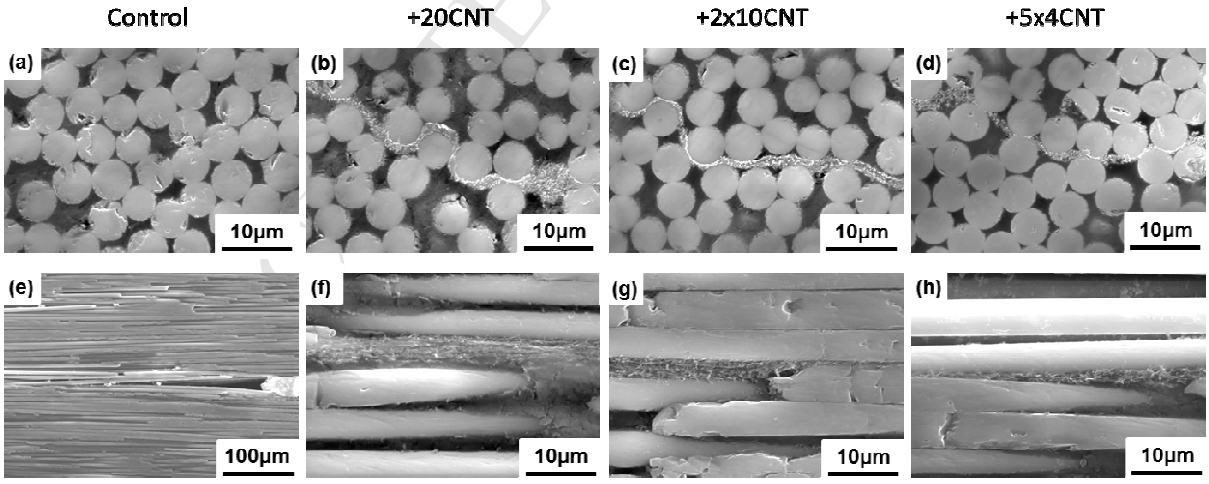

Fig. 8. SEM images of samples in 90° (a, b, c, d) and 0° (e, f, g, h) directions with different CNT web interlayer distributions: (a, e) control sample without CNT interlayer, (b. f) with one 20 layer CNT web, (c, g) with two 10 layer CNT web, (d, h) with five 4 layer CNT web.

For the electrical conduction, the CNT web interlayer provides efficient low energy paths for the electrons which contribute to the resistance reduction. The phenomenon is more obvious for the composites with the CNT web interlayer in direct contact with the copper buses where Cu-CF and CF-CF conduction is less important. As seen in the SEM images (Fig. 8), CNTs extend continuously between the carbon fibre/epoxy laminates, which provide an efficient pathway for the electrons between the two electrodes.

4. Conclusions

Composite specimens were manufactured under low and high curing pressure, and the carbon fibre volume fraction increased by 8.8% and 11.1% for //HP and ⊥HP samples respectively. Increasing the cure pressure and adding CNT web interlayers improves the electrical and thermal conductivities of the composite specimens and can be used to adjust the conductive properties of the heating element, to make the resistive heating more efficient. In addition, the carbon fibre direction has a dominant influence on heating efficiency and thermal distribution. For CF⊥Cu samples, current flows along fibres, and the resistance of the sample is low, while the resistance of the CF - Cu bus contact is relatively high. More heating occurs at the electrodes and heat spreads readily outside the heated zone. For CF//Cu samples, current must travel from fibre to fibre, the resistance of the sample is high, while the resistance of the electrode contact is relatively low. Heating occurs between the electrodes and does not spread readily outside the centre zone. Composites with CNT interlayers, especially the ones with direct contact with the copper buses, show higher electrical conductivity, while the thermal conductivity does not change significantly as a result of the different conduction modes. The number of layers comprising the CNT webs and their location in the CF structure, and hence the resistance and heating profile can be varied with ease and with virtually no weight or

volume penalty as the areal mass of a single CNT web in this work is only approximately 0.019 g/m^2 compared with the CF single prepreg layer of around 393 g/m^2. This study provides a number of parameters that can be used to create and adjust an efficient electro-thermal element in which the heat can be generated at a level and location as required.

Acknowledgments

This project has received funding from the European Union's Framework Programme 7 under the Marie Curie Career Integration Grant agreement number 630756. The authors are grateful to Dr David Thornhill and Dr Alastair Long for their IR camera support, and Dr. Thomas Dooher at NIACE for the TGA support. The corresponding author would like to acknowledge the financial support of Bombardier and the Royal Academy of Engineering.

References

[1] Napier D, Son. Electro-thermal heating system for protection of aircraft and ships against icing. Polar Record 1960; 10(64):68–70.

[2] Bragg MB, Gregorek GM, Lee JD. Airfoil aerodynamics in icing conditions. J Aircraft 1986; 23:76–81.

[3] Borrell B. How does ice cause a plane to crash? Scientific American 2009; Feb 17.

[4] McConnell VP. Past is prologue for composite repair. Reinforced Plastics 2011; 55(6):17–21.

[5] Liu HT, Hua J. Three-dimensional integrated thermodynamic simulation for wing anti-icing system. J Aircraft 2004; 41(6):1291–7.

[6] Buschhorn ST, Lachman N, Gavin J, Wardle BL. Electrothermal icing protection of aerosurfaces using conductive polymer nanocomposites. 54th AIAA/ASME/ASCE/AHS/ASC

Structures, Structural Dynamics, and Materials Conference, Boston, MA, USA, 2013; April 8-11:1-8.

[7] Falzon BG, Robinson P, Frenz S, Gilbert B. Development and evaluation of a novel integrated anti-icing/de-icing technology for carbon fibre composite aerostructures using an electro-conductive textile. Composites Part A 2015; 68:323–35.

[8] Mohseni M, Amirfazli A. A novel electro-thermal anti-icing system for fiber-reinforced polymer composite airfoils. Cold Reg Sci Technol 2013; 87:47–58.

[9] Brampton CJ, Bowen CR, Buschhorn ST, Lee J, Pickering SG, Wardle BL, et al. Actuation of bistable laminates by conductive polymer nanocomposites for use in thermal-mechanical aerosurface de-icing systems. 55th AIAA/ASME/ASCE/AHS/ASC Structures, Structural Dynamics, and Materials Conference, National Harbor, MD, USA, 2014; January 13-17:1-9.

[10] Zhao W, Li M, Zhang Z, Peng H. Carbon nanotubes based composites film heater for de-icing application. 14th European Conference on Composite Materials, Budapest, Hungary, 2010; June 7-10:1-8.

[11] Chu H, Zhang Z, Liu Y, Leng J. Self-heating fiber reinforced polymer composite using meso/macropore carbon nanotube paper and its application in deicing. Carbon 2014; 66:154–63.

[12] Kim T, Chung DDL. Carbon fiber mats as resistive heating elements. Carbon 2003; 41:2436–40.

[13] Dalili N, Edrisy A, Carriveau R. A review of surface engineering issues critical to wind turbine performance. Renew Sust Energ Rev 2009; 13:428–38.

[14] Guo P, Zheng Y, Wen M, Song C, Lin Y, Jiang L. Icephobic/anti-icing properties of micro/nanostructured surfaces. Adv Mater 2012; 24:2642–8.

[15] Wang T, Zheng Y, Raji ARO, Li Y, Sikkema WKA, Tour JM. Passive anti-icing and active deicing films. ACS Appl Mater Interfaces 2016; 8:14169–73.

[16] Zhang Z, Chen B, Lu C, Wu H, Wu H, Jiang S, et al. A novel thermo-mechanical anti-icing/de-

icing system using bi-stable laminate composite structures with superhydrophobic surface. Compos Struct 2017; 180:933–43.

[17] Nino GF, Bersee HEN, Beukers A, Ahmed TJ. Erosion of fiber reinforced thermoplastic composite structures. 49th AIAA/ASME/ASCE/AHS/ASC Structures, Structural Dynamics, and Materials Conference, Schaumburg, IL, USA, 2008; April 7-10:1–10.

[18] Parent O, Ilinca A. Anti-icing and de-icing techniques for wind turbines: Critical review. Cold Reg Sci Technol 2011; 65:88–96.

[19] Hung CC, Dillehay ME, Stahl M. A heater made from graphite composite material for potential deicing application. NASA TM 88888 1987; January 12-15:1-15.

[20] Luo J, Lu H, Zhang Q, Yao Y, Chen M, Li Q. Flexible carbon nanotube/polyurethane electrothermal films. Carbon 2016; 110:343–9.

[21] Burton B, Heintz AM, Bosworth K, Duong T, Jansen M. Uniform heat distribution in resistive heaters for anti-icing and de-icing. US Patent 0221680, 2016.

[22] Janas D, Koziol KK. Heating using carbon nanotube-based heater elements. US Patent 0366005, 2015.

[23] Janas D, Koziol KK. Rapid electrothermal response of high-temperature carbon nanotube film heaters. Carbon 2013; 59:457–63.

[24] Lee J, Stein IY, Kessler SS, Wardle BL. Aligned carbon nanotube film enables thermally induced state transformations in layered polymeric materials. ACS Appl Mater Interfaces 2015; 7:8900–5.

[25] Lu H, Liang F, Gou J, Min Huang W, Leng J. Synergistic effect of self-assembled carbon nanopaper and multi-layered interface on shape memory nanocomposite for high speed electrical actuation. J Appl Phys 2014; 115:064907.

[26] Li YL, Kinloch IA, Windle AH. Direct spinning of carbon nanotube fibers from chemical vapor deposition synthesis. Science 2004; 304:276–8.

[27] Pozegic TR, Hamerton I, Anguita J V., Tang W, Ballocchi P, Jenkins P, et al. Low temperature

growth of carbon nanotubes on carbon fibre to create a highly networked fuzzy fibre reinforced composite with superior electrical conductivity. Carbon 2014; 74:319–28.

[28] Huynh CP, Hawkins SC. Understanding the synthesis of directly spinnable carbon nanotube forests. Carbon 2010; 48:1105–15.

[29] Atkinson KR, Hawkins SC, Huynh C, Skourtis C, Dai J, Zhang M, et al. Multifunctional carbon nanotube yarns and transparent sheets: Fabrication, properties, and applications. Physica B 2007; 394:339–43.

[30] Musameh M, Notivoli MR, Hickey M, Kyratzis IL, Gao Y, Huynh C, et al. Carbon nanotube webs: A novel material for sensor applications. Adv Mater 2011; 23:906–10.

[31] Polis DL, Sovinski MF. Determination of fiber volume in carbon / cyanate ester composites using thermogravimetric analysis (TGA). NASA 2007; TM–214143: 1-9.

[32] Han S, Chung DDL. Increasing the through-thickness thermal conductivity of carbon fiber polymer-matrix composite by curing pressure increase and filler incorporation. Compos Sci Technol 2011; 71:1944–52.

[33] Hartnett JP. Advances in heat transfer, Volume 37. Academic Press. eBook ISBN: 9780080493558; 2003:202-204.